

Characterizing dynamical transitions by statistical complexity measures based on ordinal pattern transition networks

Min Huang,¹ Zhongkui Sun,² Reik V. Donner,^{3,4} Jie Zhang,⁵ Shuguang Guan,^{1, a)} and Yong Zou^{1, b)}

¹⁾School of Physics and Electronic Science, East China Normal University, Shanghai 200062, China

²⁾Department of Applied Mathematics, Northwestern Polytechnical University, Xi'an 710072, China

³⁾Department of Water, Environment, Construction and Safety, Magdeburg–Stendal University of Applied Sciences, Breitscheidstraße 2, 39114 Magdeburg, Germany

⁴⁾Potsdam Institute for Climate Impact Research (PIK) – Member of the Leibniz Association, Telegrafenberg A31, 14473 Potsdam, Germany

⁵⁾Institute of Science and Technology for Brain-Inspired Intelligence, Fudan University, Shanghai 200433, China

(Dated: 12 February 2021)

Complex network approaches have been recently emerging as novel and complementary concepts of nonlinear time series analysis which are able to unveil many features that are hidden to more traditional analysis methods. In this work, we focus on one particular approach: the application of ordinal pattern transition networks for characterizing time series data. More specifically, we generalize a traditional statistical complexity measure (SCM) based on permutation entropy by explicitly disclosing heterogeneous frequencies of ordinal pattern transitions. To demonstrate the usefulness of these generalized SCMs, we employ them to characterize different dynamical transitions in the logistic map as a paradigmatic model system, as well as real-world time series of fluid experiments and electrocardiogram recordings. The obtained results for both, artificial and experimental data demonstrate that the consideration of transition frequencies between different ordinal patterns leads to dynamically meaningful estimates of SCMs, which provide prospective tools for the analysis of observational time series.

PACS numbers: 05.45.Ac, 05.45.Tp, 89.75.Fb

In the recent decade, the field of nonlinear time series analysis has been undergoing fast developments benefiting from concepts from complex network theory. Along this line of research, ordinal pattern transition networks have been expanding the established concept of ordinal time series analysis and provide new insights into the dynamical organization underlying time series data that complement existing methods like permutation entropy. Permutation based on ordinal patterns are a simple and easy to implement concept that naturally provides statistical complexity measures (SCMs), which in the case of permutation entropy rely on pattern frequencies only. Yet, much additional information can be exploited by including order pattern transition frequencies into the definitions of SCMs – an idea that however has not been widely developed and applied so far. In this work, we generalize existing permutation based SCMs by means of ordinal pattern transition networks which take into account the pattern transition properties explicitly. The usefulness of our generalizations is demonstrated by using time series of both, model and experimental data.

I. INTRODUCTION

Complex network approaches¹ have recently emerged as prominent tools for nonlinear time series analysis^{2,3} and already found many interesting applications to observational and experimental data from various fields. In this line of research, there exist several major methods that are of particular practical importance, including cycle networks⁴, recurrence networks^{5,6}, visibility graphs^{7,8}, and transition networks^{9,10}. Depending on the particular questions at hand, each of these complex network approaches exhibit various variants that can be employed for different application purposes. For instance, we may either construct a single network representing a univariate time series, or interacting, multiplex or multi-layer networks for coupled time series. For a recent systematic review, see Ref.¹. In this work, we focus on constructing ordinal pattern transition networks (OPTNs) derived from time series data, which present the advantage of an easy implementation and a wide range of existing applications to data from different origins, including correlated stochastic processes, neurophysiological (electroencephalogram, EEG) and human cardiac activity (electrocardiogram, ECG) series^{10–15}.

The basic idea behind the OPTN method originates from identifying ordinal patterns in time series¹⁶, which is a well developed concept in nonlinear time series analysis leading to, for instance, the widely employed measure of permutation entropy¹⁶. In addition, ordinal symbolic representations of time series have found a number of interesting applications in science and engineering, for instance, in biomedi-

^{a)}corresponding author: sgguan@phy.ecnu.edu.cn

^{b)}corresponding author: yzou@phy.ecnu.edu.cn

cal recordings¹⁷, finance¹⁸, and even climate¹⁹. Some recent progress has been comprehensively reviewed in Ref.¹⁷.

Given a one-dimensional time series $\{x_i\}_{i=1,\dots,L}$ comprising L observations from a dynamical system, we first reconstruct the corresponding phase space by time delay embedding $\vec{x}_i = [x_i, x_{i+\tau}, \dots, x_{i+(D-1)\tau}]$ with an embedding dimension D ^{2,20}. Next, we represent each embedding vector \vec{x}_i by the corresponding rank order of its components, which is encoded into a symbol π_i indicating the corresponding ordinal pattern. Hence, when sliding windows from $i = 1$ to $N = L - (D - 1)\tau$ in the embedding space, a symbolic representation $\{\pi_i\}_{i=1,\dots,N}$ of the trajectory is produced. It is possible to derive information about the dynamics of the underlying system by assessing the probabilities of occurrence of different ordinal patterns. For example, for time series resulting from deterministic dynamical systems, certain patterns may not occur at all^{18,21–23}. More generally, we obtain an empirical probability distribution P whose elements p_{π_i} are the frequencies associated with the different patterns π_i , $i = 1, \dots, D!$. Clearly, P provides a significant and feasible way to estimate a characteristic probability distribution function for a given time series, which plays a crucial role in extracting statistical complexity information on the underlying dynamical system^{16,17}.

The conceptually relatively simple estimation of P based on ordinal patterns for the underlying system prompts to another successful application of this framework in terms of statistical complexity measures (SCMs)²⁴. One common way of defining SCMs is taking the product of a normalized Shannon entropy and an associated measure of disequilibrium^{24,25}, which captures specific organizational properties of structure and patterns in the observed process. Following the vast amount of previous work on this topic^{24–27}, we consider here a variant of SCMs based on the concept of Jensen-Shannon divergence, which is defined as $C_{JS}[P] = \mathcal{H}[P] \cdot Q_{JS}[P, P_e]$, where $\mathcal{H}[P]$ is the normalized Shannon entropy and $Q_{JS}[P, P_e]$ is the so-called disequilibrium function measuring the distance of the given distribution P to the uniform distribution P_e . Accordingly, we define $Q_{JS}[P, P_e] = Q_0 \cdot JS[P, P_e]$ where $JS[P, P_e]$ is the Jensen-Shannon divergence between P and P_e and Q_0 is a normalization factor. Furthermore, the complexity–entropy plane $\mathcal{H} \times C_{JS}$ has been widely used to distinguish chaotic systems from stochastic ones²⁶. The analysis of complexity–entropy planes has already taken advantage from the ordinal pattern based symbolic encoding of time series and has found various applications^{24,26}. However, in the classical complexity–entropy analysis, there are some chaotic maps that could be easily confused with random noise because no clearly separable domains of values are available to differentiate those different types of dynamics as reported in Ref.¹⁴. So far, it remains a challenging task to disclose a possible non-monotonic relationship between complexity and entropy²⁸.

It may be noted that in the context of symbolic dynamics based time series analysis methods, the transition behavior between patterns has already been discussed as early as in Ref.²⁹, where the authors introduced the concept of fluctuation complexity. However, in combination with ordinal pat-

terns, the corresponding idea has long remained not being systematically exploited, especially from a time series network perspective. Recently, OPTN representations have been proposed to precisely capture this transition behavior of the ordinal patterns^{10–14}, which opens a broader perspective beyond the standard ordinal symbolic analysis of time series. In this framework, each ordinal pattern is considered as a vertex in a graph, and a directed and weighted edge connecting two patterns in the graph is established according to the corresponding transition frequency (i.e., the probability with which a given permutation is followed by a certain other one). One of the advantages of the resulting OPTNs is that we can obtain a pronounced distinction between different types of systems based on short time series only^{10,14}.

In this work, we draw upon the recent success of both, complexity–entropy plane analysis and OPTNs, to generalize existing SCMs by incorporating pattern transition probabilities. The advantages of this approach, which will be demonstrated in the course of this work, are as follows: (i) The modified SCMs allow for a clear distinction between different types of dynamics, which is demonstrated for time series from numerical models and experimental data. (ii) The generalized SCMs help to capture a consistent relationship between SCMs and chaoticity. (iii) All SCMs are sensitive to dynamical transitions along a bifurcation scenario, including period doubling, band merging, inner and outer crises.

The remainder of this paper is organized as follows: In Section II, we introduce the methodology employed in our work. We start by discussing two slightly different ways to obtain the transition matrix between ordinal patterns, which provides the basis for defining the corresponding OPTNs (Section II A). Based on this matrix, we propose in Section II B to compute SCMs from three different perspectives, including static pattern frequency properties, dynamic pattern transition properties, and a combination of both. In Section III, we proceed with describing some selected results for the logistic map as a paradigmatic model system exhibiting various types of periodic and chaotic solutions. We first discuss in some detail one example of a periodic orbit to emphasize the important effects of the embedding dimension in Section III A. The practical usefulness of SCMs will be further illustrated by studying four exemplary time series from different typical dynamical regimes (Section III B). In Section III C, the complexity–entropy planes associated with each SCM will be discussed as the control parameter of the logistic map is systematically varied. In order to characterize the dynamical transitions in this model, we further study the behavior of the SCM values in dependence on the control parameter in Section III D and show that similar results can also be obtained for time-continuous dynamical systems like the Rössler oscillator in Section III E. Finally, we demonstrate that SCMs successfully distinguish different dynamical regimes in experimental time series from flow data and human ECG measurements in Section IV. Some concluding remarks and discussions will be provided in Section V.

II. METHODS

A. Ordinal pattern transition matrix

Most recent studies employing the concept of permutation entropy \mathcal{S}_O have defined this measure by focusing exclusively on the frequencies of ordinal patterns, which however disregards the transition behavior between subsequent patterns. To emphasize on the transition frequencies between any pair of patterns, measures of transitional complexity have been further proposed in Refs.^{12,13} to quantify the properties of the associated OPTNs. To this end, we associate each directed link in an OPTN with a transition frequency $w_{ij} = p_{\pi_i \rightarrow \pi_j}$. Calculating the transition frequencies for each pair of patterns, we hence obtain a weighted and directed network characterized by a weighted adjacency matrix $\mathbf{W} = \{w_{ij}\}$ with $i, j \in \{1, \dots, D!\}$.

Based on this transition matrix \mathbf{W} of an OPTN, we note that there are two slightly different ways to introduce normalization factors. The first option¹² is to use a global normalization to ensure that $\sum_{i,j}^{D!} w_{ij} = 1$, which results in a globally normalized transition entropy as discussed below. The second option has been proposed by McCullough *et al.*¹³ who considered the local out-link transition frequency from pattern π_i to π_j

$$p_{\pi_i \rightarrow \pi_j} = \begin{cases} 0, & \text{if } \pi_i = \pi_j \\ \frac{w_{ij}}{\sum_{j,j \neq i} w_{ij}}, & \text{if } \pi_i \neq \pi_j. \end{cases} \quad (1)$$

Note that the transition frequency of Eq. (1) is pattern (row) wise normalized. This case will be referred to as the node-wise out-link normalized transition matrix \mathbf{W} in the following. In this way, it easily captures the heterogeneous behavior of both, (static) occurrence frequencies of different patterns and (dynamic) transition frequencies between patterns.

In addition to the proper normalization, we need to consider self-loops that may affect the numerical estimation of \mathbf{W} especially for time series from continuous systems with a given sampling rate. For example, it has been demonstrated in Ref.¹² that there are about 99% self-loops in time series of the Rössler system when integrated with a step size $h = 0.01$, while the about 1% non-self-loops are hidden in \mathbf{W} . From this example, one may easily see that self-loops are related to the serial correlation of the time series under study¹⁴. **From the viewpoint of statistical measures of complex network theory**, neglecting self-loops in \mathbf{W} emphasizes the transition behavior between different patterns, which has therefore been adopted in most existing studies of complex networks for computational simplicity and theoretical concerns³⁰. Accordingly, we also remove self-loops in the present study before computing \mathbf{W} while acknowledging that in other cases of **highly correlated** stochastic processes and discrete systems, self-loops have been included in the analysis showing some interesting results^{14,31}. Arguably, whether to remove or to consider self-loops depends on the particular process under study. In any of the applications discussed in the rest of this paper, our results do not change qualitatively when including self-loops

(see Supplementary Material Sec. SM1 with Figs. S1 to S3 for some illustrative examples).

B. Statistical complexity measures

In the following, we briefly review the existing ordinal pattern frequency based SCM before proposing two **alternatives** to define SCMs, which explicitly consider transition frequencies of the resulting OPTN representations for time series.

1. SCM based on the permutation entropy of pattern frequencies

The permutation entropy of a time series is the Shannon entropy of the distribution of patterns $P = \{p_{\pi_1}, p_{\pi_2}, \dots, p_{\pi_{D!}}\}$, which is defined as

$$\mathcal{S}_O[P] = - \sum_{i=1}^{D!} p_{\pi_i} \log p_{\pi_i}. \quad (2)$$

The normalized permutation entropy \mathcal{H}_O hence follows as

$$\mathcal{H}_O[P] = \mathcal{S}_O[P]/\mathcal{S}_{O,max}, \quad (3)$$

where $\mathcal{S}_{O,max} = \log D!$ corresponds to the case of a uniform distribution of the same number of patterns, i.e., $P_e = \{1/D!, \dots, 1/D!\}$.

In the next step, we use some appropriate statistical concept to measure the distance of the empirical distribution P to a uniform distribution P_e , which is the essential idea behind the class of SCMs considered in this work. Several different distance functions have been employed in the literature, including the Euclidean norm, Wooters' distance, Kullback-Leibler relative entropy and Jensen-Shannon divergence²⁴. In this work, the distance between the distributions P and P_e is characterized by the Jensen-Shannon divergence $Q_{JS}[P] = Q_0 \cdot JS[P, P_e]$ with

$$JS[P, P_e] = \mathcal{S}_O[(P + P_e)/2] - \frac{1}{2} \mathcal{S}_O[P] - \frac{1}{2} \mathcal{S}_O[P_e], \quad (4)$$

where Q_0 is a normalization factor with equals the inverse of the maximal Jensen-Shannon divergence $JS[P, P_e]$, which ensures that $Q_{JS}[P] \in [0, 1]$. This maximal distance is obtained when the distribution P has probability one for one pattern and zero for all other patterns. The general expression for Q_0 reads

$$Q_0 = \frac{-2}{\left(\frac{M+1}{M}\right) \log(M+1) - 2 \log(2M) + \log(M)}, \quad (5)$$

where $M = D!$ is the total number of possible patterns. For large D , we have $Q_0 \approx 1/\log 2$.

The function $Q_{JS}[P]$ is different from zero if the system has a kind of preference of certain patterns among the accessible ones, reflecting determinism of the system. Finally, the

SCM based on permutation entropy estimated from the empirical node (pattern) frequencies is defined as

$$\mathcal{C}_O[P] = Q_{JS}[P] \cdot \mathcal{H}_O[P]. \quad (6)$$

This quantity is static in the sense that it quantifies the amount of information stored by ordinal pattern frequencies in the system and its disequilibrium of the observed parts of its accessible states in comparison to a uniform distribution²⁵.

2. SCM based on the transition entropy of the globally normalized weight matrix

In this case, the sum of all entries of the transition matrix \mathbf{W} is 1, and the Shannon entropy of transition frequencies between any pair of ordinal patterns is therefore

$$\begin{aligned} \mathcal{S}_W[W] &= - \sum_{i=1}^{D!} \sum_{j=1; j \neq i}^{D!} w_{ij} \log w_{ij}, \\ &= - \sum_{i=1}^{D!} \sum_{j=1; j \neq i}^{D!} p_{\pi_i \rightarrow \pi_j} \log p_{\pi_i \rightarrow \pi_j}. \end{aligned} \quad (7)$$

The normalized entropy is hence defined

$$\mathcal{H}_W[W] = \mathcal{S}_W[W] / \mathcal{S}_{W,max}, \quad (8)$$

where $\mathcal{S}_{W,max} = \log D!(D! - 1)$ as any self transitions are excluded. Furthermore, there are $D!(D! - 1)$ possible pattern transitions in the uniform distribution function P_e . If self-loops are considered in the transition matrix, the normalization factor $\mathcal{S}_{W,max} = \log D! \cdot D!$ is used instead and there are at most $D!^2$ possible pattern transitions in P_e .

In full analogy with the permutation entropy based SCM, the Jensen-Shannon divergence is computed as $Q_{JS}[W] = Q_0 \cdot JS[W, P_e]$ with

$$JS[W, P_e] = \mathcal{S}_W[(W + P_e)/2] - \frac{1}{2} \mathcal{S}_W[W] - \frac{1}{2} \mathcal{S}_W[P_e]. \quad (9)$$

We note that we have the same expression for the normalization factor Q_0 as above when setting $M = D!(D! - 1)$ in Eq. (5). This further yields the SCM

$$\mathcal{C}_W[W] = Q_{JS}[W] \cdot \mathcal{H}_W[W]. \quad (10)$$

This quantity is dynamic in the sense that it considers the state transition information stored in the system.

3. SCM based on the transition entropy of the node-wise out-edge normalized weighting matrix

We finally consider the case where the ordinal pattern transition matrix is node-wised normalized, i.e., the row sum of \mathbf{W} is 1. Accordingly, we again first introduce the node-wise

out-link transition entropy

$$\begin{aligned} \mathcal{S}_E^{\pi_i}[W_{\pi_i}] &= - \sum_{j=1; j \neq i}^{D!} w_{ij} \log w_{ij}, \\ &= - \sum_{j=1; j \neq i}^{D!} p_{\pi_i \rightarrow \pi_j} \log p_{\pi_i \rightarrow \pi_j} \end{aligned} \quad (11)$$

and node-wise normalized transition entropy

$$\mathcal{H}_E^{\pi_i}[W_{\pi_i}] = \mathcal{S}_E^{\pi_i}[W_{\pi_i}] / \mathcal{S}_{E,max} \quad (12)$$

with $\mathcal{S}_{E,max} = \log(D! - 1)$. Note that this normalization factor is the same for all patterns, i.e., $\mathcal{S}_{E,max}^{\pi_i} = \mathcal{S}_{E,max}^{\pi_j}$. Therefore, the superscript index can be suppressed in the above definition. If self-loops are considered in the transition matrix, the normalization factor $\mathcal{S}_{E,max} = \log D!$ is used.

In addition, the node-wise Jensen-Shannon divergence is defined as $Q_{JS}^{\pi_i}[W_{\pi_i}] = Q_0 \cdot JS^{\pi_i}[W_{\pi_i}, P_e]$ with the disequilibrium measure

$$\begin{aligned} JS^{\pi_i}[W_{\pi_i}, P_e] &= \\ \mathcal{S}_E^{\pi_i}[(W_{\pi_i} + P_e)/2] - \frac{1}{2} \mathcal{S}_E^{\pi_i}[W_{\pi_i}] - \frac{1}{2} \mathcal{S}_E^{\pi_i}[P_e]. \end{aligned} \quad (13)$$

In this case, we obtain the normalization factor Q_0 by setting $M = D! - 1$ in Eq. (5). Taking into account node frequencies, the global Jensen-Shannon divergence is computed as

$$Q_{JS}[W, P_e] = \sum_{i=1}^{D!} p_{\pi_i} Q_{JS}^{\pi_i}[W_{\pi_i}], \quad (14)$$

which therefore yields an alternative definition of an SCM of the OPTN as

$$\mathcal{C}_E[W] = Q_{JS}[W, P_e] \cdot \mathcal{H}_E[W], \quad (15)$$

where $\mathcal{H}_E[W] = \sum_i p_{\pi_i} \mathcal{H}_E^{\pi_i}[W_{\pi_i}]$. This quantity is dynamic in the sense that it takes both the static ordinal pattern frequencies and the dynamic state transition information into account.

C. Practical considerations

One important practical aspect of the proposed methodology concerns the data requirements for computing entropies and complexity measures. It is easily understandable that a higher value of the embedding dimension D is generally preferable since it leads to a larger variety of ordinal patterns and, hence, a more robust statistics over the frequencies of such patterns. On the other hand, in order to sample all possible patterns sufficiently, this implies the requirement of increasingly longer time series as D rises. For a reliable estimation of the classical SCMs from symbolic dynamics that are based on pattern frequencies only, a pragmatic condition suggested in the literature would be considering time series of a length L that is sufficiently larger than $D!$ ^{26,32} (e.g., $N > 5D!$).

The situation becomes even more challenging when our modified SCMs are considered, since they are based on transition frequencies instead of pattern frequencies. For $D!$ different ordinal patterns for embedding dimension D , there may exist $D!^2$ possible source–destination pairs. However, if we consider $\tau = 1$ and transitions corresponding to shifting the time index by one time step only, it is clear that from the D components of the source permutation, $D - 1$ also contribute to the corresponding destination pattern without changing their mutual order relationships^{14,31}. Hence, the new state contributing to the destination pattern can only lead to at most D different ordinal patterns, i.e., we have at most $D \cdot D!$ different pattern transitions. However, for other cases like $\tau > 1$ and/or larger time shifts between ordinal patterns to be considered, up to $D!^2$ different pairs of patterns and, hence, transitions could occur in the worst case. In general, we conclude that the far higher number of pattern transitions as compared to patterns themselves puts severe restrictions to the choice of D in practical applications of the new SCMs in the context of time series of a given length L .

III. NUMERICAL EXAMPLES

A. Effect of embedding parameters

There are two important algorithmic parameters in constructing OPTNs – the embedding parameters D and τ . The choice of D and τ can markedly affect the results for the associated SCMs since D and τ should compromise the essential time scales of the dynamics in the underlying time series. In common applications of ordinal pattern analysis (e.g., the estimation of the permutation entropy S_O), the choice of optimal (or just pragmatic) values of D and τ depends on the field of application as systematically summarized in Ref.³³. Throughout the remainder of this work, we will consider D as a free parameter, which is varied in the range of $D \in \{2, \dots, 7\}$, although for the sake of brevity, we will mainly show the results for $D = 6$ as illustration. The associated choice of the embedding delay τ is commonly less crucial in nonlinear time series analysis methods. In our numerical examples discussed below, the corresponding selection will be mainly guided by the attempt to highlight the fact that lower entropy values are expected for periodic as compared to chaotic behavior. In order to cope with a single parameter only, we will particularly use $\tau = D$ for the artificial (deterministic and stochastic) model systems considered in the following, independent of the particular value of D . We emphasize that this choice is not based on specific considerations of performance optimization, but simply reflects convenience and serves solely illustrative purposes. Two examples for results obtained with $D = 6$ and $\tau = 1$ for two well-known model systems can be found in the Supplementary Material Sec. SM2, Figs. S4 and S5.

As an illustrative example highlighting the important roles of D and τ for ordinal pattern based time series analysis, we consider a period-4 solution of the logistic map

$$x_{i+1} = rx_i(1 - x_i) \quad (16)$$

with $r = 3.5$. In this example, the choice of $\tau = D$ reflects the particular role of specific choices of the embedding parameters in the context of low-order periodic windows (here, period-4 and period-3) in the bifurcation sequence of the logistic map. As expected, Fig. 1 demonstrates that the resulting ordinal pattern sequences are significantly affected by the different parameter settings, which further result in different permutation entropy values H_O . For instance, only one unique ordinal pattern is observed when $\tau = D = 4$ (Fig. 1(c, g)) resulting in $H_O = 0$, which is due to the coverage of exactly one full period by the particular embedding parameters. Other values of D and τ however yield non-zero entropy values. The results of Fig. 1 may raise concern since different choices of D and τ will change the placement of the system in the complexity–entropy plane. In the special case of the logistic map, we do not have a unique choice of D and τ for all different periodic windows when the control parameter r is varied. When the control parameter r is changed, we should rather focus on the transitions between different dynamical regimes.

B. Results for four typical dynamical regimes

We further illustrate the potential of the proposed SCMs to characterize the logistic map with the control parameter r varying in the range $[3.5, 4]$ with a step size of $\Delta r = 0.001$. In this range of r , various dynamical regimes and transitions between them can be found, for instance, period doubling cascades, band merging points, inner and outer crises, and intermittency², which has made this system serving as a paradigmatic model for assessing nonlinear time series analysis methods⁵.

As a first step, we consider four representative regimes that can be observed at particular values of the control parameter r , corresponding to either periodic dynamics or chaotic dynamics close to band merging, in some laminar state, and at the outer crisis. In all examples, we will consistently use the embedding parameters $D = \tau = 6$. In the following, we will use realizations of the logistic map comprising $L = 10^6$ iterations (after removing the first 1000 iterations of each realization which might reflect transient behavior of the system before reaching its respective attractor), which meets the conditions for the necessary time series length for $D = 6$ as discussed in Sect. II C.

For all four situations, we investigate the SCMs along with their dual entropy characteristics in detail and summarize the obtained results in Tab. I. We note that several types of chaos–chaos transitions will be discussed in the following: the band merging crisis corresponds to intermittency, the inner crisis to some more subtle chaos–chaos transition and the outer crisis to fully chaotic dynamics.

Due to our specific choice of τ and D , all SCMs take values of zero for the period-3 series because the temporal distance between each pair of components of the embedding vector covers a multiple of two full periods (cf. Fig. 1). Other choices of D and τ would commonly yield non-zero values for the period-3 regime. For the three other cases of band merging,

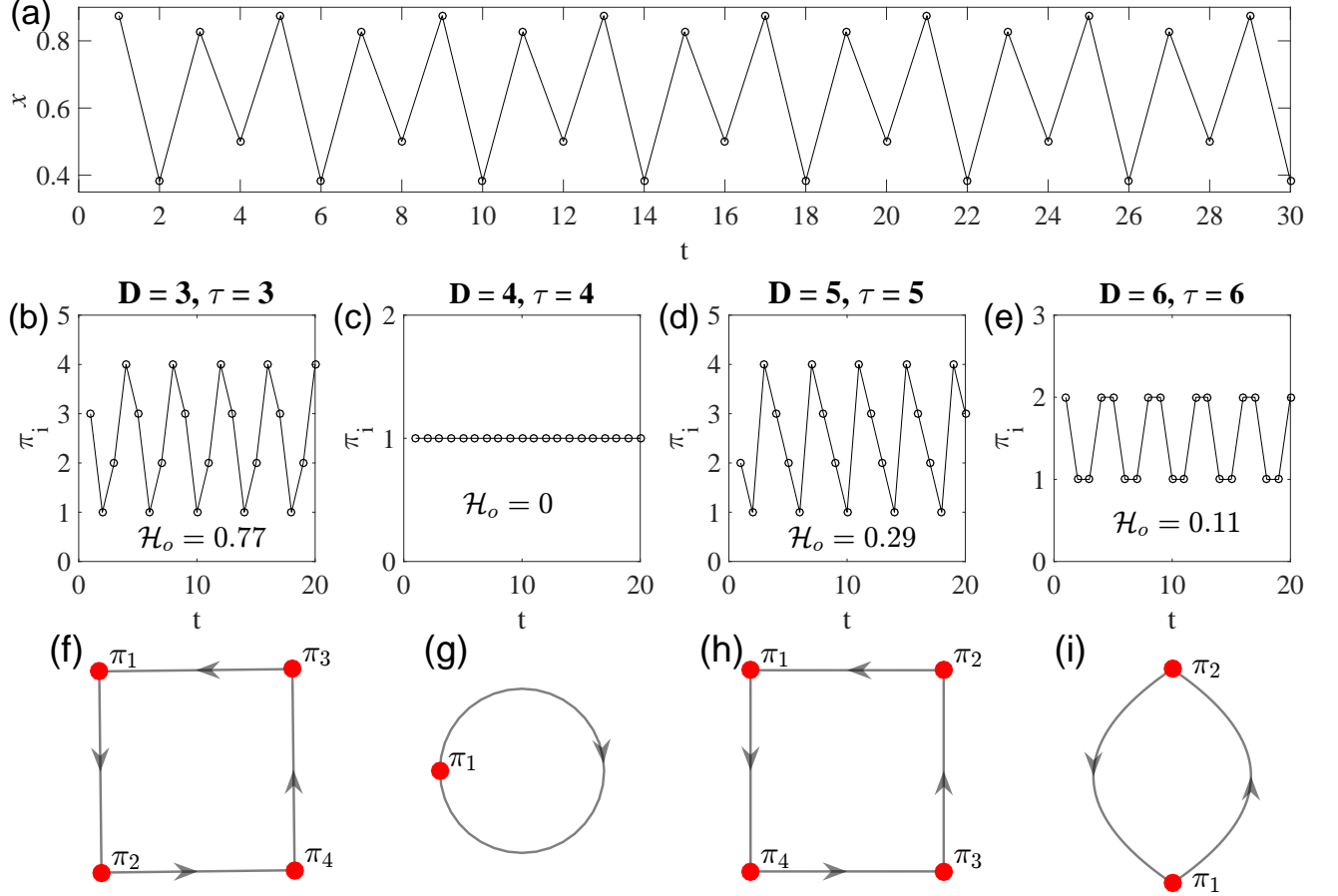


FIG. 1. Example of a period-4 time series demonstrating the effects of different choices of the embedding parameters D and τ . (a) Time series comprising 30 iterations of the period-4 orbit. The corresponding ordinal pattern series are shown for different combinations of D and τ **selected for illustrative purposes**: (b) $\tau = D = 3$, (c) $\tau = D = 4$, (d) $\tau = D = 5$, and (e) $\tau = D = 6$. The respective permutation entropy values normalized by $\log D!$ as in Eq. (3) are indicated in the insets of each panel. Panels (f)-(i) show the corresponding OPTNs. The weights of directed edges are not shown (recall that two slightly different normalizations are considered in this work). Note that in panel (g), there exist exclusively self-loops since $\tau = D = 4$ results in a unique, constant pattern. Missing patterns are suppressed.

Regime	r	\mathcal{H}_O	\mathcal{C}_O	\mathcal{H}_W	\mathcal{C}_W	\mathcal{H}_E	\mathcal{C}_E
period-3	3.83	0	0	0	0	0	0
band merging	3.679	0.978	0.043	0.639	0.582	0.302	0.277
laminar state	3.791	0.989	0.026	0.671	0.618	0.354	0.328
outer crisis	4.0	1.0	0	0.761	0.662	0.522	0.458

TABLE I. Values of the three considered SCMs along with their adjoint entropy measures for four different values of the control parameter r of the logistic map (embedding parameters: $D = \tau = 6$).

laminar state and outer crisis, the values of all SCMs significantly differ from zero. The pattern frequency based SCM \mathcal{C}_O shows zero value and $\mathcal{H}_O = 1$, which implies a positioning in the lower right corner of the complexity–entropy plane in Fig. 2(a). However, for the transition matrix based SCMs, both the estimated entropies \mathcal{H}_W , \mathcal{H}_E and associated complexity measures \mathcal{C}_W , \mathcal{C}_E show results that are more consistent

with the expectations when considering the respective level of chaoticity of the system in those three regimes (i.e., a rising Lyapunov exponent with increasing r in the respective chaotic regimes). In particular, the estimated SCMs take their largest values for $r = 4$ in the outer crisis regime, and the SCMs are the smallest when $r = 3.679$ in the band merging case, while the laminar regime displays intermediate SCM values.

C. Complexity–entropy planes

1. Logistic map

In order to put our previous results into a broader context, we next show the complexity–entropy planes obtained when varying the control parameter r in the logistic map. This simple nonlinear system has already been widely discussed in the framework of SCMs^{28,34}, but only for pattern frequency based complexity measures. For each value of r , we again construct

OPTNs from time series of length $L = 10^6$ with the embedding parameters $D = \tau \in \{2, \dots, 7\}$. As far as the classical ordinal pattern frequency based SCM is concerned, the given time series length is compatible with the chosen range of D values, while the largest embedding dimension of 7 is at the edge of the range where the “optimistic” estimate in Sec. II C can be considered to apply for transition frequency based SCMs as well.

In the context of finite sample size effects, we note that for the particular example of the logistic map, one could easily generate realizations of much longer lengths. Our numerical results show, however, that longer realizations of a length of up to $L \leq 5 \cdot 10^6$ do not change the obtained entropy and SCM estimates significantly (not shown). From a practical perspective, two aspects call for attention in interpreting the obtained entropy and SCM values quantitatively. On the one hand, due to the finite numerical precision of the computed trajectories, any chaotic regime may in fact turn out to appear as periodic (with arbitrarily long periods); this can lead to numerical artifacts that will be further discussed in Sec. III D. On the other hand, all estimated values of the different entropy and complexity measures always need to be considered as finite sample estimates that may well deviate from their expected asymptotic values and thereby depend on the specific values of L and D available for the analysis. This is, however, a feature that is also common to other existing symbolic dynamics based entropies and SCMs.

As another introductory side note, we recall that as already stated above, when only one unique ordinal pattern is identified in a given time series, all SCMs take a value of 0, which is reasonable since only self-loops are observed. This however happens only if the embedding parameters are chosen such that they exactly coincide with the periodicity of a certain periodic window (see Fig. 1(g)). Hence, it cannot be expected that a given fixed choice of the embedding parameters will be able to highlight all periodic windows of arbitrary order in exactly the same quantitative way.

In previous works, SCMs have been applied to distinguish chaos from noise by employing the concept of complexity–entropy plane²⁶. Generalizing this idea to our OPTN based SCMs, we can define three such planes showing the statistical complexity measures (C_O , C_W and C_E) as a function of the corresponding normalized entropy values (\mathcal{H}_O , \mathcal{H}_W and \mathcal{H}_E). The three SCMs characterize both randomness and correlation structure in a time series, which as a consequence results in a non-trivial dependence on the associated entropy values. Specifically, chaotic systems present high complexity while stochastic systems have lower values of complexity, hence ideally appearing in distinct regions of the complexity–entropy plane²⁶. Furthermore, it has been shown previously that at a given entropy value, the range of possible SCM values is bound by a minimum C_{min} and a maximum C_{max} . A general algorithm for computing these bounds has been provided in Ref.³⁵.

Figure 2 shows the complexity–entropy planes for embedding parameters $D = \tau$ varied between 4 and 6. We emphasize that the results are qualitatively similar for $D = \tau = 3, 7$ as well (not shown). Furthermore, it is notable that the val-

ues of C_{max} depend on the embedding dimension D since D determines the number of patterns and pattern transitions which are considered in the definition of SCMs. Along with the specific results for the logistic map, Fig. 2 also shows the theoretical limiting curves of C_{min} and C_{max} for three different embedding dimensions ($D = 4, 5, 6$). While the lower bounds show only little variation with increasing D , the upper limits are more strongly affected and gradually shift upward for larger embedding dimensions.

As a first general observation, we recover the known result that the established pattern frequency based SCM values for the logistic map lie close to the theoretical maximum C_{max} for a given entropy value (Fig. 2(a, d)), while some residual variation of the displacement of the estimated values from those upper bounds is retained for all considered values of the embedding dimension D . Most notably, we find many combinations of complexity–entropy values in the lower right part of the plane (high entropy, low complexity), which is commonly indicative of stochastic processes and has been visually highlighted by rectangles of dotted lines. This region of the plane is challenging for SCMs to distinguish between chaotic time series and random noise¹⁴ and is in our case occupied by values corresponding to chaotic regimes of the logistic map at large r values. The corresponding ambiguity results from the fact that both \mathcal{H}_O and C_O only take static information into account in the sense that only pattern frequencies have been considered in their definitions. The observed behavior confirms previous findings that distinguishing (especially high-dimensional) chaotic from stochastic dynamics can be a challenging task in established ordinal pattern based time series analysis methods^{17,33}.

For our new pattern transition based SCMs, we find that in the complexity–entropy planes $\mathcal{H}_W \times C_W$ and $\mathcal{H}_E \times C_E$, the results for the logistic map again closely align with the theoretical upper bounds C_{max} . When increasing the embedding dimension, the estimated values approach the theoretical C_{max} curve more and more closely, implying that the SCM values are (almost) completely determined by the underlying entropy values as D becomes large. For C_E and \mathcal{H}_E the obtained SCM values align particularly closely with C_{max} already at low embedding dimensions (Fig. 2(c, f)). We hypothesize that this is due to the fact that the definition of these characteristics takes information on both, pattern frequencies and transition frequencies into account, while the other two complexity–entropy pairs focus on only one if those two aspects.

More importantly, for sufficiently large D the resulting complexity–entropy pairs essentially cover exclusively the left uprising branch of the curve for the SCM accounting for transition frequencies (Figs. 2(b, e) and 2(c, f)), which distinctively differs from the original permutation entropy based SCM. In this regard, one may note that this branch implies an almost linear dependency between C_W and \mathcal{H}_W (Fig. 2(e)), respectively, C_E and \mathcal{H}_E (Fig. 2(f)), which especially applies for small entropy values within an increasingly wide range as D increases. This linear increase of the maximum complexity versus entropy curve for sufficiently large embedding dimension is expected from theoretical considerations³⁶. Some

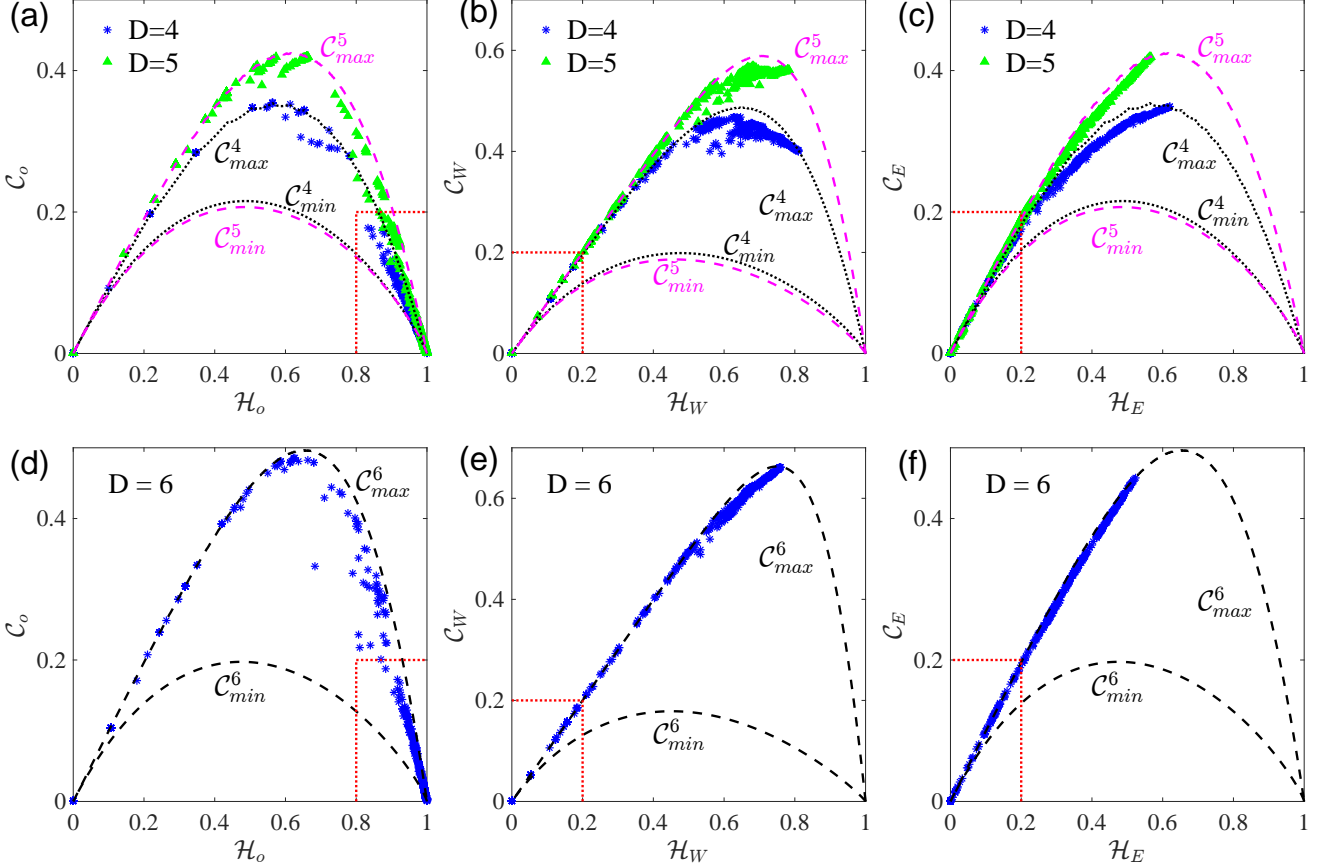


FIG. 2. (Color online) Three different complexity–entropy planes (based on the Jensen-Shannon divergence) illustrating the behavior of the three SCMs for example series of the logistic map with varying control parameter r : (a, d) \mathcal{C}_O versus \mathcal{H}_O , (b, e) \mathcal{C}_W versus \mathcal{H}_W , and (c, f) \mathcal{C}_E versus \mathcal{H}_E . The dotted lines correspond to \mathcal{C}_{max} and \mathcal{C}_{min} in dependence on the respective entropy for $D = 4$ (panels a-c), and the dashed lines indicate \mathcal{C}_{max} and \mathcal{C}_{min} for $D = 5$ (a-c) and $D = 6$ (d-f), respectively. In panels (a, d), the bottom-right rectangles of dotted red lines indicate the regions for the traditional pattern frequency based SCM analysis where the differentiation between stochastic and deterministic–chaotic dynamics is ambiguous. However, the lower left rectangles of (b, c, e, f) correspond to regions of lower complexities.

more discussions have been provided in the Supplementary Material (Sec. SM3, Fig. S6-S8).

In our opinion, the most interesting result is, however, that we do not find any complexity–entropy pairs in the lower right part of the plane, which for the classical SCM based on permutation entropy would present the challenging region of possible ambiguity between deterministic-chaotic and stochastic dynamics. By contrast, we find many values in the lower left corner of the plane showing small values of both, \mathcal{C}_W and \mathcal{C}_E (Fig. 2(b, c, e, f)). This region of the complexity–entropy plane may be indicative of regular (periodic) orbits with low complexity. As already emphasized above, along with the choice of embedding parameters, the length of time series and the finite computational precision play important roles in the practical estimation process, possibly mimicking regular behavior in case of actually chaotic dynamics, which could be a reason for the unexpected population of the lower left part of the complexity–entropy planes. The mentioned numerical effects will be further discussed in Sec. III D. Starting out of both, the lower left and right corners, the transition frequency based SCMs \mathcal{C}_W and \mathcal{C}_E show consistent trends along with

the degree of chaoticity, as will also be detailed in Sec. III D below. Taken together, we suggest that the deterministic transition behavior among patterns allows an improved distinction from random noise as compared to pattern frequency based approaches.

The behavior of the different SCMs relative to their respective lower and upper bounds can be further highlighted by considering normalized quantities. Specifically, for a given \mathcal{H} and D , we define a normalized complexity $\mathcal{C}^N = (\mathcal{C} - \mathcal{C}_{min}) / (\mathcal{C}_{max} - \mathcal{C}_{min})$, which is theoretically bound to the interval $[0, 1]$. Large values of those normalized complexities close to 1 indicate a good alignment with the maximum complexity curve. The corresponding results for the logistic map are shown in Fig. 3. As expected, for the traditional \mathcal{C}_O , the behavior is characterized by many points in the right half plane (large entropies, see Fig. 3(a)) for all considered embedding dimensions. In contrast, there are no points in the range of $\mathcal{H} > 0.8$ for \mathcal{C}_W and \mathcal{C}_E (Fig. 3(b, c)). Note that in Fig. 3(c), some normalized complexity values larger than 1 arise at small entropies due to numerical artifacts when the control parameter r is close to a bifurcation point, which re-

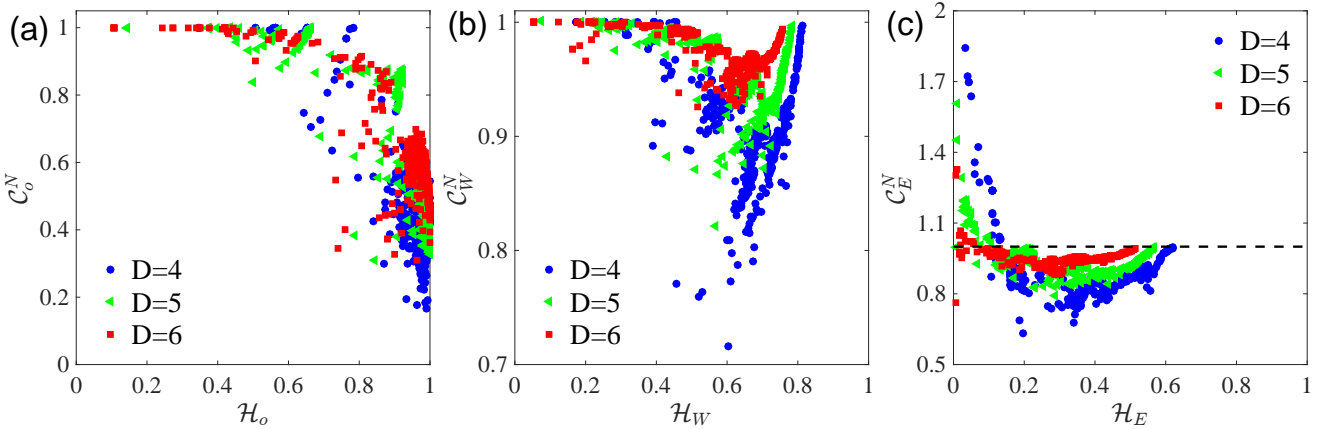


FIG. 3. (Color online) Normalized complexity – entropy planes of the three SCMs for the logistic map: (a) \mathcal{C}_O , (b) \mathcal{C}_W , and (c) \mathcal{C}_E . In (c), normalized complexity values larger than 1 indicate numerical artifacts when the control parameter r approaches a bifurcation point, resulting in long transients. The respective embedding dimensions are indicated by different colors (see legend).

sults in long transients (as will be explained in Sec. III D).

2. Fractional Brownian motion and fractional Gaussian noise

In order to further analyze the capability of our modified complexity–entropy planes to distinguish chaotic from stochastic dynamics, we next compare the results for the logistic map with those obtained for fractional Brownian motion (fBm), i.e., stochastic processes with long-range temporal correlations. Specifically, for an fBm process the long-range correlations of the process are uniquely characterized by the Hurst exponent H when positively correlated (persistence) for $1/2 < H < 1$, while being suppressed (anti-persistence) for $0 < H < 1/2$. $H = 1/2$ corresponds to the classical Brownian motion. Similar to the previous case of the logistic map with varying control parameter r , we generate time series for varying $H \in (0, 1)$ with a step size of $\Delta H = 0.05$ and present the resulting complexity–entropy planes in Fig. 4.

Moreover, since fBm series in the persistent regime are nonstationary, we further transform all fBm realizations into stationary time series by employing first-order difference filtering, i.e., by considering the increments $x_{i+1} - x_i$. The transformed series are commonly referred to as fractional Gaussian noise (fGn), and the associated complexity–entropy planes are shown in Fig. 5. Notably, fGn retains the long-range correlations and Gaussian probability density function (PDF) of the underlying fBm process. For a discussion on practical concerns regarding time delay embedding of fBm and fGn processes, we refer to Ref.³⁷.

Comparing the results for both types of stochastic processes with those for the logistic map, a few important observations are made. First of all, the traditional pattern frequency based SCM values as originally reported by Rosso and co-workers^{26,34} are well reproduced as expected (Figs. 4(a, d) and 5(a, d)). Second, unlike for the logistic map all complexity–entropy pairs of fBm and fGn clearly differ from the theoreti-

cal maximum complexity values, which is a general behavior that does not change with increasing embedding dimension D . From a more qualitative perspective, all three complexity–entropy pairs lead to parabola-shaped curves similar to those of the associated lower and upper bounds. However, it is notable that the transition based SCMs \mathcal{C}_W and \mathcal{C}_E tend to exhibit higher numerical values than \mathcal{C}_O .

Especially for the new OPTN based SCMs, we find a partial overlap between the entropy values of fBm and the logistic map, while the associated SCM values are however clearly distinct except for the fBm realizations with the lowest entropy values, which correspond to the most nonstationary situations (H close to 1). In general, we observe for all three complexity–entropy planes of fBm that with increasing D , the associated range of entropy values extends further towards the left (lower entropies). Taken both, upward and leftward shift of the complexity–entropy curves individually may therefore enhance the risk of confusing deterministic-chaotic and stochastic processes in the complexity–entropy plane even with our alternative SCMs. However, our results indicate that combining information on the position in the complexity–entropy plane and on the stationarity could allow a clear distinction between chaotic and stochastic dynamics even in extreme situations (e.g., a large value of H). Notably, for the stationary fGn, all three complexity–entropy planes are confined to very high entropy and low complexity values – a range where no combinations have been found for the new transition frequency based SCMs for the logistic map.

While we have excluded self-loops in the definitions of the considered SCMs so far, including the latter does not modify the results discussed above markedly. In the Supplementary Material Sec. SM1, Figs. S1-S3, we provide additional illustrations showing the complexity–entropy planes for fBm and fGn for this methodological variant, revealing no qualitative and only minor quantitative changes with respect to the results discussed above. This may however differ for strongly correlated deterministic systems, a type of dynamics that we have not yet investigated in the course of the present study.

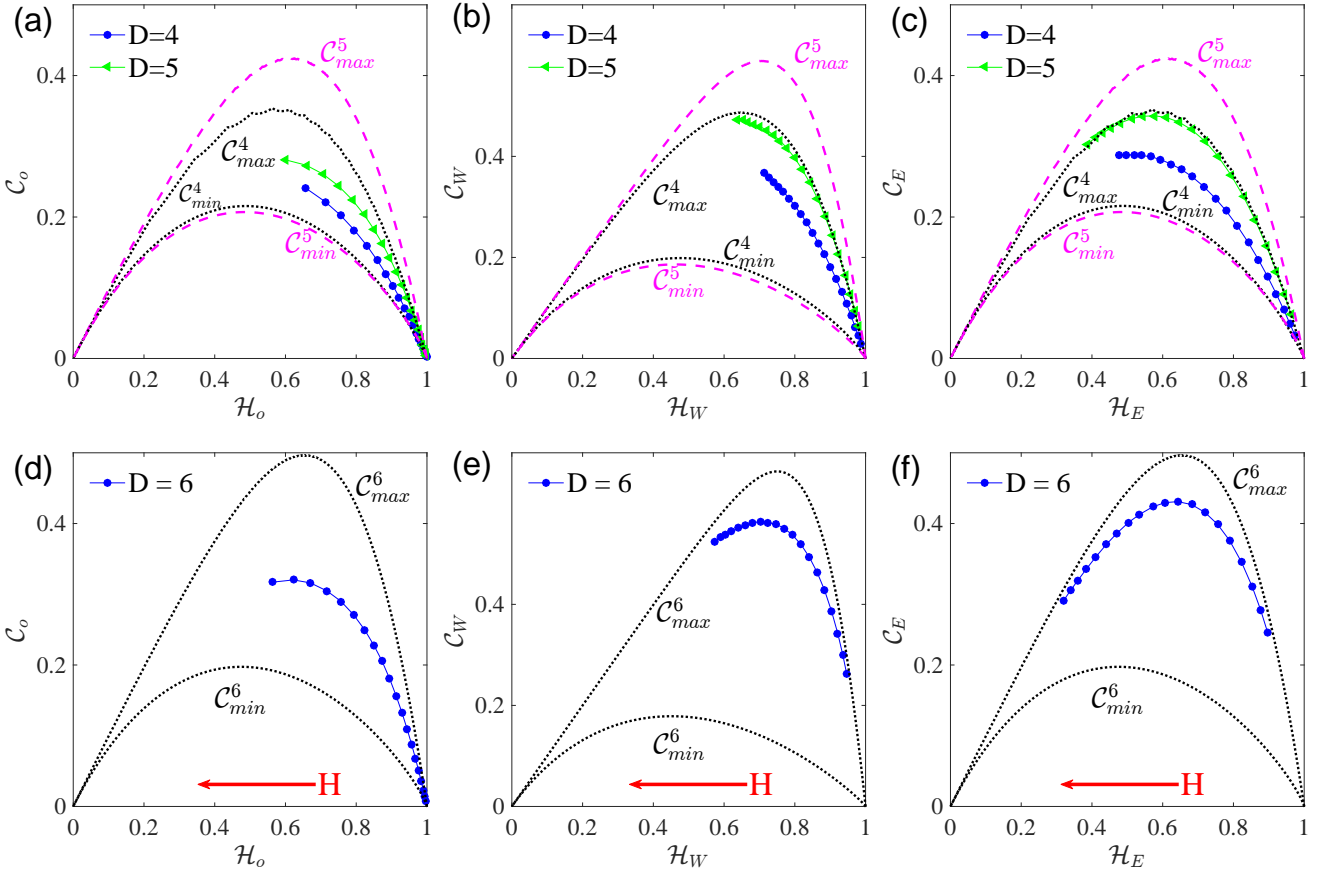


FIG. 4. (Color online) Same as in Fig. 2, but for fractional Brownian motion with a Hurst exponent $H \in (0, 1)$ varying with a step size of $\Delta H = 0.05$. Note that the normalized entropy is generally decreasing with increasing H (red arrow).

Finally, to highlight the difference in complexity values between logistic map and fBm, we show in Fig. 6 the behavior of the normalized SCMs with entropy for different embedding dimensions D . It can be seen that increasing D gradually shifts the normalized complexity values closer to 1 while at the same time allowing for gradually lower entropy values, which is consistent with the findings in the standard (non-normalized) complexity–entropy planes. However, the obtained normalized curves still deviate significantly from those previously found for the logistic map, indicating a good separation between both types of dynamics using each of the three considered SCMs.

Taken all reported results on the complexity–entropy planes for the logistic map, fBm and fGn together, we conclude that the modified SCMs indeed tend to distinguish chaotic from stochastic dynamics more precisely than the original approach. We therefore suggest that the pattern transition behavior encoded in the OPTNs provides novel insights that can be exploited in terms of SCMs that complement their traditional counterparts.

D. Characterizing dynamical transitions

The logistic map experiences a sequence of different types of bifurcations when the control parameter r is systematically increased. However, the corresponding dynamical regimes and regime transitions are not easy to identify from the complexity–entropy planes discussed above. In the following, we therefore explicitly study the dependence of our SCMs on the control parameter r . Here, our motivation is to verify whether the normalized entropies and associated SCMs computed from OPTNs are indeed able to detect the dynamical transitions along the complex bifurcation scenarios of the logistic map and hence track qualitative changes in the dynamics, including both period–chaos and chaos–chaos transitions. As a benchmark, we take the associated Lyapunov exponent as an established measure for characterizing the type of dynamics (regular versus chaotic) along with the degree of chaoticity.

As a general observation, we find that all three SCMs clearly follow the changes in the bifurcation diagram, for instance, showing distinct values in periodic windows (highlighted by grey color in Fig. 7 and Supplementary Material Fig. S4, where the obtained results are shown for the same embedding dimension $D = 6$, but two different values of the embedding delay τ). Other than C_O , the two transition fre-

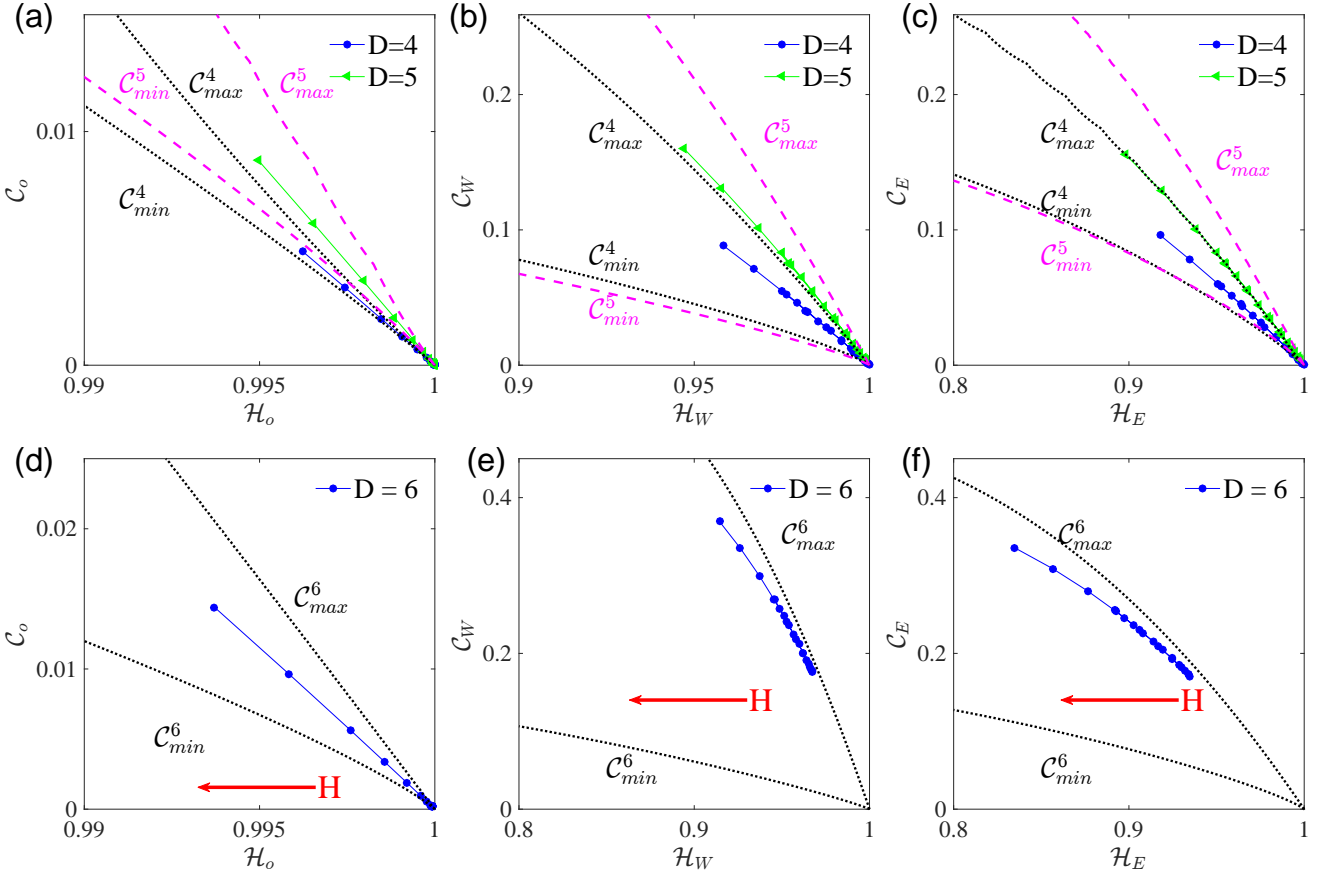


FIG. 5. (Color online) Same as in Fig. 2, but for fractional Gaussian noise with a Hurst exponent $H \in (0, 1)$ varying with a step size of $\Delta H = 0.05$. Note that only a small region of the complexity–entropy planes is covered in this case.

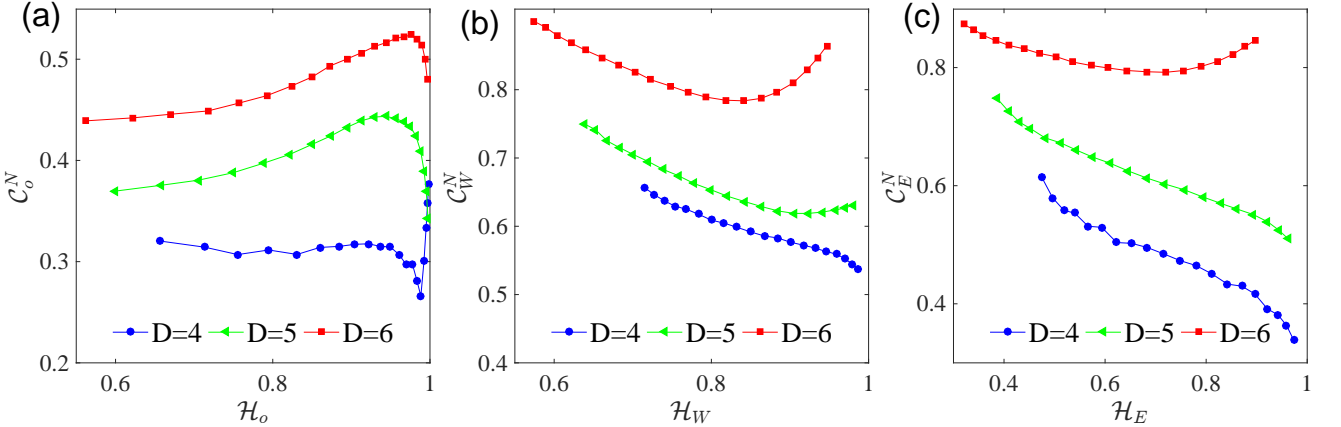


FIG. 6. (Color online) Same as in Fig. 3, but for different realizations of fractional Brownian motion with varying Hurst exponent H .

quency based SCMs behave in a similar way as the Lyapunov exponent. Specifically, as the control parameter r is increased, the chaoticity level grows gradually, reaching a maximum at $r = 4$, which is reflected by an increase in statistical complexity. A similar increase is absent in the pattern frequency based complexity measure C_O (Fig. 7(c)). In this context, we note that it is an established fact that pattern frequency

based SCMs often do not trace the growth in the chaoticity of the logistic map²⁸, which can however be improved by using Wooster's distance function instead of the Shannon-Jensen divergence employed in this work. From this point of view, the pattern transition frequency based SCMs C_W and C_E exhibit some more informative behavior in the sense that they track the growth of the level of chaoticity.

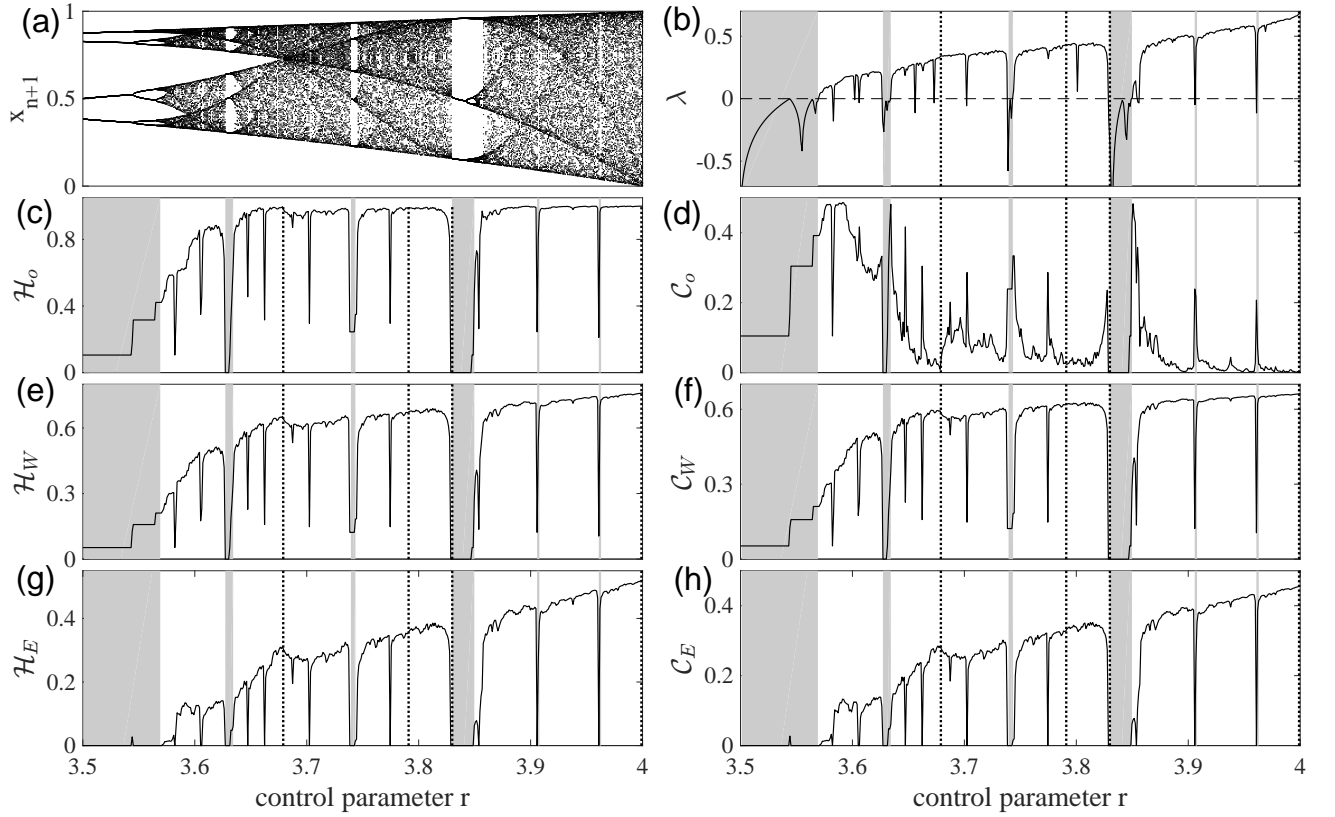


FIG. 7. Behavior of the different SCMs and associated entropy characteristics for the logistic map in dependence on the control parameter r (embedding dimension $D = 6$, embedding delay $\tau = 6$). (a) Bifurcation diagram, (b) Lyapunov exponent, (c) pattern frequency based (permutation) entropy H_O and (d) associated complexity measure C_O ; (e) pattern transition frequency based entropy H_W based on the globally normalized transition matrix \mathbf{W} and (f) the corresponding complexity measure C_W , and (g, h) entropy H_E and complexity measure C_E based on the node-wise out-link normalized transition matrix \mathbf{W} . Several major periodic windows have been highlighted by grey background shading. Vertical dotted lines indicate the cases summarized in Tab. I.

Another conceptual improvement is found for H_E and C_E in the parameter range where the logistic map presents period doubling bifurcations, for example, at $r = 3.544$ (Fig. 7(g, h)). It may be noticed that H_O , C_O , H_W and C_W all exhibit non-zero values in this parameter range despite a purely periodic dynamics. Furthermore, there are jumps of all four measures at the points of period doubling bifurcations, which have already been reported in Ref.¹⁶. These jumps however are not desirable since the complexity of the dynamics does not change when r passes any of those points. For the case of the period doubling bifurcation at $r = 3.544$ (replacing a period-4 by a period-8 solution), we show in Fig. 8 that the observed jump in the entropy and SCM values may be explained by accumulated numerical errors during the iterations attracted to the periodic-4 points, which yields long transients. For estimations based on time series of finite length as used in this work, H_E and C_E are however not affected in the same way showing much smaller values (Fig. 7(g, h)). Certainly, we should not over-interpret their capabilities since numerical inaccuracy would be accumulated in a longer iterative process such that different ordinal patterns are identified. In addition, we pass through many periodic windows of different periods as the control parameter r is varied, which prevents us from

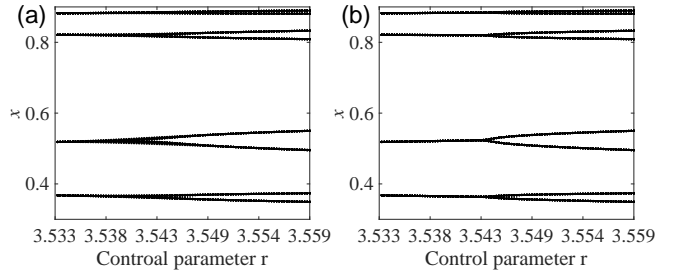


FIG. 8. Transient behavior affecting the generation of proper bifurcation diagrams for the logistic map, exemplified here for the period doubling bifurcation from a period-4 to a period-8 solution. (a) The actual bifurcation point gets blurred when r is close to 3.544 if only a short transient of 50 iterations is removed from the time series. (b) When a sufficiently large number of initial iterations (2000) are removed, the correct bifurcation point becomes visible.

using a unique predefined number of iterations as initial transients for time series with different period length. Notably, similar jumps have also been observed when the system bifurcates from a period-3 to a period-6 solution at $r = 3.842$.

E. Dynamical transitions in continuous system

While we have focused so far exclusively on the case of the time-discrete logistic map, it may be interesting to study whether a similar behavior can also be obtained for time-continuous deterministic dynamical systems. To this end, we will illustrate a corresponding analysis for the example of the chaotic Rössler system³⁸

$$\begin{aligned}\dot{x} &= -y - z, \\ \dot{y} &= x + 0.2y, \\ \dot{z} &= b + z(x - 5.7)\end{aligned}\quad (17)$$

while varying the control parameter b . From a conceptual perspective, constructing OPTNs for time series from continuous systems faces certain additional practical challenges, including the proper choice of sampling frequency and embedding parameters, which depend on the particular time scales of the system. To avoid any corresponding discussion on proper choices of further algorithmic parameters, we employ here a Poincaré section to each sample trajectory of the system at $y = 0$, $\dot{y} < 0$ (for different values of b) and construct OPTNs from $N = 10,000$ intersection points. The results are shown in Fig. 9 and Supplementary Material Fig. S5 for the same embedding dimension $D = 6$, but two different values of the embedding delay τ . Based on these results, we conclude that the general behavior of the different SCMs and associated entropy measures closely resembles that reported for the logistic map in Fig. 7. Specifically, all measures trace the succession of bifurcations in the considered range of b . We outline more detailed follow-up investigations on the behavior of our OPTN based SCMs to such time-continuous systems directly as relevant topics for future work.

IV. REAL-WORLD EXAMPLES

While we have previously demonstrated the suitability of OPTN based SCMs for tracing changes in dynamical complexity for time series from deterministic dynamical systems, in the following we will use two different sets of experimental time series to demonstrate that our SCMs also successfully characterize the complexity properties of real-world systems, showing distinct values for different types of dynamics.

The first example originates from a laboratory fluid experiment of baroclinic instability which is used to study patterns of cyclones and anticyclones in the Earth's atmosphere^{39,40}. Depending on the parameters rotation rate, temperature difference, viscosity and fluid density, this experimental system exhibits a rich variety of flow regimes. In particular, we focus on the following regimes:

- (i) Stable fluid (SW): The temperature signal of the stable flow exhibits periodic oscillations as the wave drift patterns arrive at the fixed point of measurements.
- (ii) Quasi-periodic 2-frequency amplitude vacillation (AV-2): This case is identified as a 2-frequency quasi-periodic amplitude flux. The wave drift is composed of

slow and regular oscillations in the temperature signal, but a fast modulation in the amplitude is also visible. AV-2 is characterized by a periodic growth and drop in wave amplitude with little change in waveform.

- (iii) Quasi-periodic 3-frequency amplitude vacillation (AV-3): For the sake of completeness, we also analyze a quasi-periodic 3-frequency amplitude vacillation time series. Unlike for the other studied cases, this time series has not been obtained from experimental results, but from a three-dimensional direct numerical simulation of the air-filled rotating baroclinic instability experiment³⁹.
- (iv) Modulated amplitude vacillation (MAV): This case is identified as a low-dimensional stream, chaotically modulated and with waves of varying amplitudes. Amplitude modulation results in a complex temperature dynamics.

One temperature time series of each flow regime has been measured at 2 s resolution for periods of up to $9 \cdot 10^4$ s. Therefore, each recording consists of $N = 45,000$ data points. Example segments of the resulting time series are shown in Fig. 10 for illustrative purposes. Further details on the lower-dimensional chaotic properties have been reported in Refs.^{39,41}.

The second set of example time series comprises physiological signals of human electrocardiogram (ECG) recordings collected from patients from the MIT-BIH Database and the Creighton University Cardiac Center⁴². Heart rate variability suffering from ventricular arrhythmia presents a physiologically highly significant anomaly that is still relatively poorly understood from a dynamical system perspective, showing rich nonlinear properties⁴³. The ECG recordings have been obtained at a 250 Hz sampling frequency for about 8.5 minutes⁴². From these long-term recordings, we focus on the three different rhythmic states of normal sinus rhythm (SR), ventricular tachycardia (VT) and ventricular fibrillation (VF)⁴³, which have been annotated by skilled cardiologists based on waveform morphology. To reduce possible finite-size effects in estimating SCMs, we study time series of at least 10,000 time points each. In consequence, out of 18 different patients, we obtain 14 time series showing sinus rhythm (SR) prior to the onset of arrhythmia, 12 records of VT and 17 records of VF. After the annotations, all time series have different lengths, ranging from 14600 to 159600 data points in SR, 16000 to 132000 in VT, and 14500 to 124000 in VF. We do not apply any preprocessing to the data, except for checking the length requirements. We show some segments of time series of each case in Fig. 11.

For choosing the embedding parameters for both sets of example time series, we follow the suggestions from earlier studies^{40,43}. Although we are facing the inevitable presence of nonstationarity and noise in the experimental data, we have verified that the following results do not change qualitatively as the embedding parameters are varied. In particular, we have again treated the embedding dimension as a free parameter, which has been varied in the range of $D = 2, 3, \dots, 6$. In turn, the embedding delay τ has been fixed as determined by the first root of the autocorrelation function². In the case of the

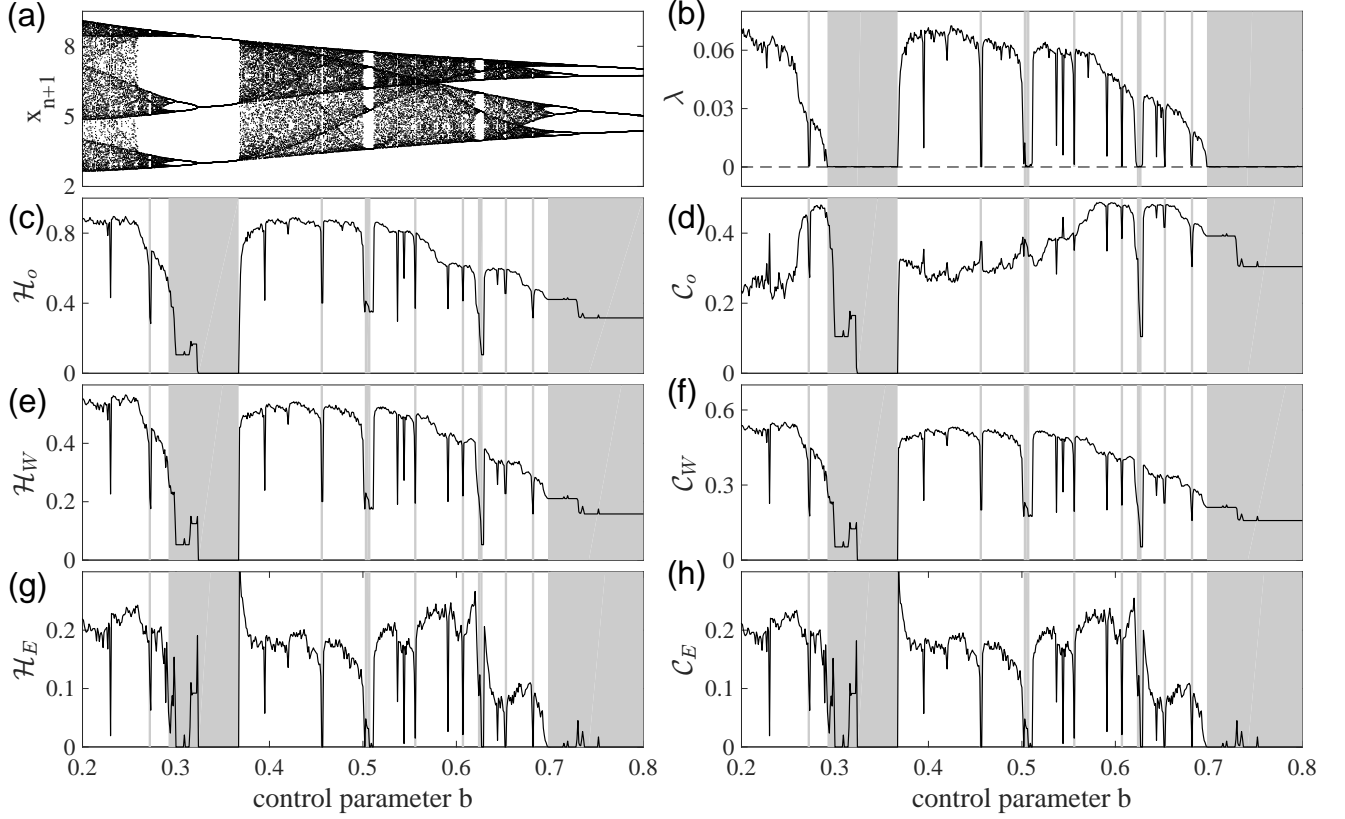


FIG. 9. Same as Fig. 7, but for Poincaré sections of the Rössler system while varying the control parameter b (see text for details, **embedding dimension $D = 6$**). Panel (a) presents a bifurcation diagram based on the x components of all points in the Poincaré sections. Panel (b) shows the largest Lyapunov exponent of the system in dependence of b .

temperature time series from the fluid experiments, $\tau_1 = 110$ time steps (data points) for SW, AV-2 and AV-3, while $\tau_2 = 60$ for MAV, which is consistent with the existing literature^{39,41}. For the ECG time series, we consistently use an embedding delay of $\tau = 5$ time steps as suggested in Refs.⁴³. The results have been aggregated over all subjects.

In both sets of time series, the OPTN based SCMs enhance our understanding of the underlying nonlinear system, which can be seen from the results summarized in Figs. (12, 13). For the fluid data (Fig. 12), \mathcal{H}_O , \mathcal{H}_W , \mathcal{C}_W , \mathcal{H}_E and \mathcal{C}_E all show consistent changes of the complexity and entropy values between stable wave solution (SW), quasi-periodic 2-frequency amplitude vacillation (AV-2), quasi-periodic 3-frequency amplitude vacillation (AV-3) and chaotic modulated amplitude vacillation (MAV). Specifically, the complexity of these four cases has the following order: SW has the lowest complexity since it shows periodic oscillations with trivial recurrence, while MAV has the highest complexity since it presents chaotically modulated amplitude vacillation. Quasiperiodic states exhibit intermediate complexity values since these two cases have non-trivial recurrences while still featuring a certain degree of regularity. In our case, AV-3 presents a higher complexity than AV-2, which should however be interpreted with care since the AV-2 series originates from an experiment, while the AV-3 series has been taken from a numerical simulation of the same system (hence, there may be a certain level of

observational noise present in AV-2 but not in AV-3). The order of complexity values between periodic, quasiperiodic and chaotic solutions still holds for \mathcal{C}_O , but the corresponding values become very similar. In particular, it becomes hard for \mathcal{C}_O to identify the difference between AV-2 and AV-3.

Qualitatively similar results are obtained for the ECG recordings, as shown in Fig. 13 for three different embedding dimensions. Generally speaking, different ECG recordings exhibit remarkably distinct complexity values since the ensemble medians are well separated between different time series groups of SR, VF and VT as shown by the box plots in Fig. 13. More specifically, SR recordings show very pronounced the highest median of \mathcal{H}_O , \mathcal{H}_W , \mathcal{C}_W , \mathcal{H}_E and \mathcal{C}_E , reflecting the existence of significant spectral power in a rather broad frequency band between 50 and 100 beats/min in the signals⁴³. On the other hand, the complexity of VT has the smallest value, even lower than for the case of VF. Unlike the other five measures, we note, however, that SR shows the smallest median values of \mathcal{C}_O while VT has the largest values (Fig. 13(b)).

Meanwhile, we find a mild dependence of the discriminatory power of \mathcal{C}_O and \mathcal{C}_W on the embedding dimension D . In particular, in the case of $D = 6$ the median values of \mathcal{C}_O of VF are comparable to that of VT (Fig. 13(b)). On the other hand for $D = 4$, the median values of \mathcal{C}_W are all comparable for SR, VF and VT (Fig. 13(d)). This insufficiency of

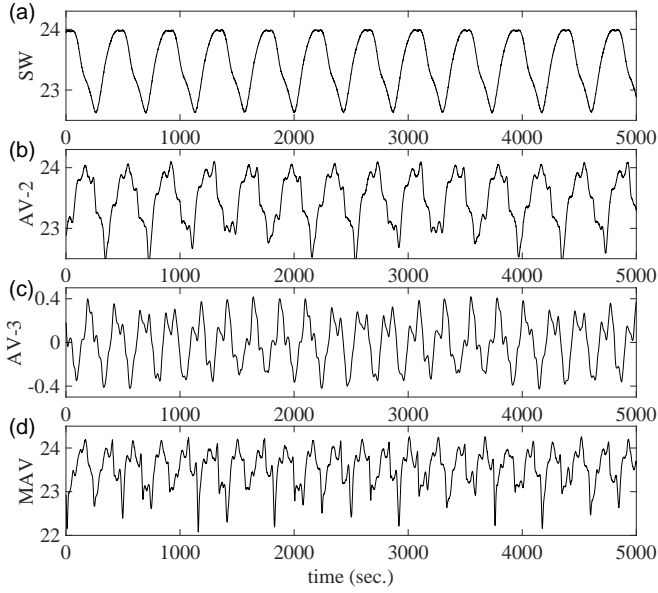


FIG. 10. Sample segments of the temperature recordings from the flow experiment: (a) SW, (b) AV-2, (c) AV-3 and (d) MAV. The vertical axis describes the temperature T .

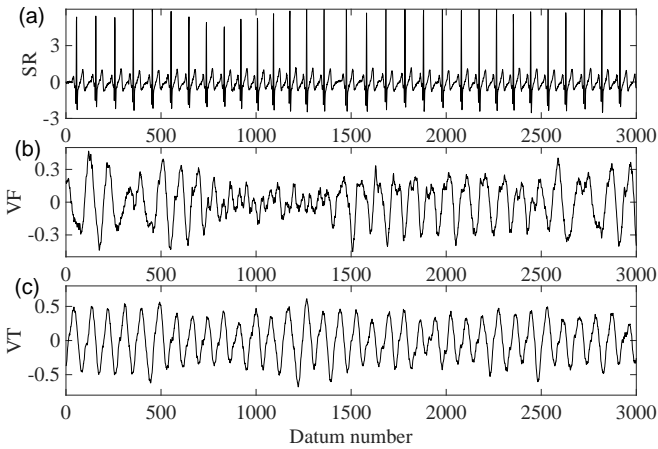


FIG. 11. Three representative ECG recording sections (randomly chosen from different rhythmic states): (a) sinus rhythm (SR), (b) VF and VT. The horizontal axis of each panel is the datum number (at 250 Hz sampling rate) and the vertical axis describes the ECG surface voltage (in mV).

C_O and C_W to detect differences in case of improper embedding dimension may be explained by the fact that C_O takes only static pattern frequencies into account, while C_W considers dynamic pattern transitions, which may therefore not be able to properly distinguish subtle differences reflected in the temporal order of patterns. In contrast, C_E considers both individual pattern frequencies and dynamic pattern transition frequencies.

V. CONCLUSIONS

In summary, we have proposed to expand the traditional ordinal pattern frequency analysis by also including ordinal pattern transitions, thereby generalizing existing statistical complexity measures for nonlinear time series analysis. The pattern transition properties encoded in the underlying time series networks allow to gain insights beyond those provided by the celebrated permutation entropy method which relies on the pattern frequencies only. Therefore, this study presents another case showing the usefulness of applying ordinal pattern transition networks for time series analysis¹.

We have suggested two slightly different ways to incorporate the effects of pattern transitions in statistical complexity measures, which are based on (i) a globally normalized transition matrix and (ii) a node-wise normalized transition matrix. Here, the complexity measure based on the node-wise normalized matrix combines both, individual pattern frequencies and the frequencies of transitions among patterns. We have shown that the associated two new statistical complexity measures characterize the complexity properties of deterministic chaos successfully and clearly highlight deterministic-chaotic dynamics in the corresponding complexity–entropy planes (Fig. 2). This finding helps to obtain an improved complexity analysis for time series of both, deterministic chaos and stochastic systems, fostering their better discrimination. However, further more systematic numerical performance tests employing different types of dynamical systems are required to provide compelling evidence for distinctions between different types of dynamics beyond the cases presented in the current work^{14,34}. While this opens several opportunities for follow-up research, we have already demonstrated here the practical usefulness of our improved SCMs by employing this framework to time series of experimental fluid flows and ECG recordings, showing statistically significant discriminatory power for different cases.

Some open problems also common to other nonlinear time series analysis methods remain to be further addressed, for example, the dependence of reliable estimates of SCMs on the available time series length. For reliable estimations of traditional entropy \mathcal{H}_O and SCM C_O , a minimum time series length of $L > 5D!$ has been largely suggested^{16,17}. However, even much longer lengths are required for the newly proposed SCMs based on transition frequencies, since the transition matrix has the dimensions $D! \cdot (D! - 1)$ if self-loops are excluded. This should however not present a problematic issue when working with time series from numerical models provided with the rapidly increasing computing power nowadays. For time-discrete dynamical systems like chaotic maps, one may easily generate longer data series, which however does not necessarily improve the estimates very much due to the accumulation of effects resulting from a limited numerical precision (Fig. 8). The dependence of the new SCMs on the time series length L becomes crucial for experimental time series studies. One interesting problem in this context is to understand the extra information of transition probability based complexity measures since strong linear correlations have been found between complexity and entropy at small en-

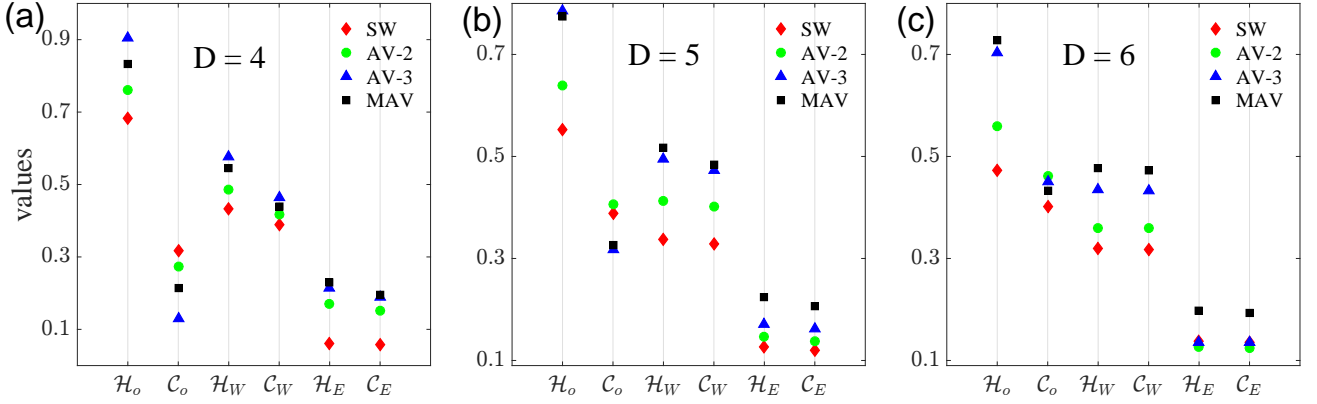


FIG. 12. OPTN based entropy and SCM characteristics for experimental fluid data, which are shown for embedding dimensions of $D = 4, 5, 6$. In all subfigures, stable wave (SW, ♦), quasiperiodic 2-frequency amplitude vacillation (AV-2, ●), quasiperiodic 3-frequency amplitude vacillation (AV-3, ▲) and chaotic modulated amplitude vacillation (MAV, ■) are distinguished.

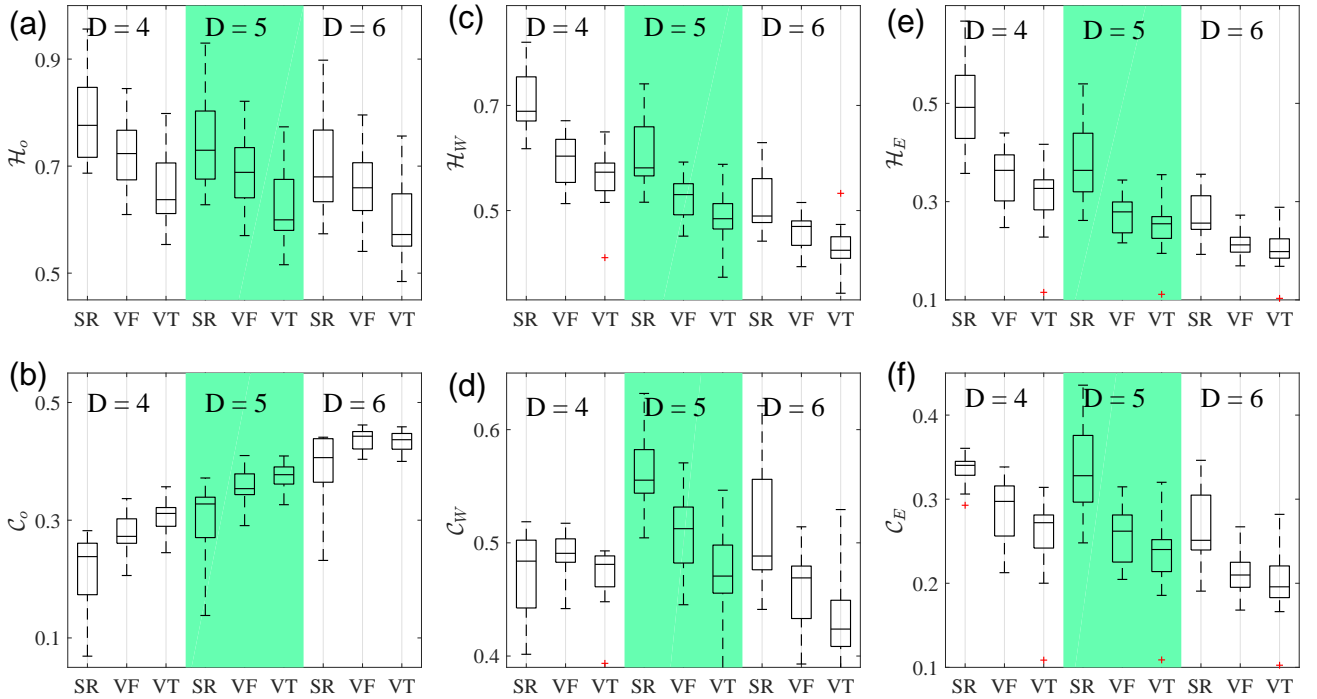


FIG. 13. Box plots for OPTN based entropy and SCM characteristics for human ECG recordings, showing well separated medians for each subject group SR, VF and VT. Entropy and SCM scores are shown for embedding dimensions of $D = 4, 5, 6$.

tropy values, which are expected for a large number of patterns (i.e., $M = D!$) for high embedding dimension D (or, in a similar spirit, $M = D! \cdot (D! - 1)$ transitions). For continuous systems, together with the embedding parameters, the sampling frequency is another important characteristic which needs to be further explored. Moreover, the generalization of our approach from univariate to bivariate time series analysis shall be further discussed. We noticed that this aspect has remained a largely untouched subject for statistical complexity analysis so far, while it presents an interesting task to show the dependence of complexity on interaction. Finally, it appears an interesting aspect to integrate some of the established

higher-order network topological characteristics into the definition of additional SCMs, for instance, clustering coefficients or average path lengths, which have been widely discussed to characterize the dynamical properties of the system generating the time series at hand¹. We outline further work on the aforementioned topics as subjects of future research.

ACKNOWLEDGEMENTS

Parts of this work have been financially supported by the National Natural Science Foundation of China (grant no.

11872182, 11835003, 11875132, 61973086), the Natural Science Foundation of Shanghai (grant no. 18ZR1411800). JZ and YZ further acknowledge support by the Shanghai Municipal Science and Technology Major Project (grant no. 2018SHZDZX01) and ZJ Lab. The authors thank J. B. Borges and O. A. Rosso for sharing algorithms for computing C_{min} and C_{max} , and two anonymous reviewers for helpful comments on the original version of this manuscript.

DATA AVAILABILITY STATEMENT

The fluid data that support the findings of this study are available from the corresponding author upon reasonable request. The ECG data that support the findings of this study are openly available in <https://www.physionet.org> from MIT-BIH Database and the Creighton University Cardiac Center⁴².

- ¹Y. Zou, R. V. Donner, N. Marwan, J. F. Donges, and J. Kurths, “Complex network approaches to nonlinear time series analysis,” *Physics Reports* **787**, 1–97 (2019).
- ²H. Kantz and T. Schreiber, *Nonlinear Time Series Analysis*, 2nd ed. (Cambridge University Press, Cambridge, 2004).
- ³J. C. Sprott, *Chaos and Time-Series Analysis* (Oxford University Press, Oxford, 2003).
- ⁴J. Zhang and M. Small, “Complex network from pseudoperiodic time series: Topology versus dynamics,” *Phys. Rev. Lett.* **96**, 238701 (2006).
- ⁵N. Marwan, J. F. Donges, Y. Zou, R. V. Donner, and J. Kurths, “Complex network approach for recurrence analysis of time series,” *Phys. Lett. A* **373**, 4246–4254 (2009).
- ⁶R. V. Donner, Y. Zou, J. F. Donges, N. Marwan, and J. Kurths, “Recurrence networks — a novel paradigm for nonlinear time series analysis,” *New J. Phys.* **12**, 033025 (2010).
- ⁷L. Lacasa, B. Luque, F. Ballesteros, J. Luque, and J. C. Nuno, “From time series to complex networks: The visibility graph,” *Proc. Natl. Acad. Sci.* **105**, 4972–4975 (2008).
- ⁸A. Nuñez, L. Lacasa, J. Patricio, and B. Luque, “Visibility Algorithms: A Short Review,” in *New Front. Graph Theory* (InTech, 2012) Chap. 6, pp. 119–152.
- ⁹G. Nicolis, A. G. Cantu, and C. Nicolis, “Dynamical aspects of interaction networks,” *Int. J. Bifurc. Chaos* **15**, 3467–3480 (2005).
- ¹⁰M. McCullough, M. Small, T. Stemler, and H. H.-C. Iu, “Time lagged ordinal partition networks for capturing dynamics of continuous dynamical systems,” *Chaos* **25**, 053101 (2015).
- ¹¹C. W. Kulp, J. M. Chobot, H. R. Freitas, and G. D. Sprechini, “Using ordinal partition transition networks to analyze ECG data,” *Chaos* **26**, 073114 (2016).
- ¹²J. Y. Zhang, J. Zhou, M. Tang, H. Guo, M. Small, and Y. Zou, “Constructing ordinal partition transition networks from multivariate time series,” *Scientific Reports* **7**, 7795 (2017).
- ¹³M. McCullough, M. Small, H. H. C. Iu, and T. Stemler, “Multiscale ordinal network analysis of human cardiac dynamics,” *Philos. Trans. R. Soc. A Math. Phys. Eng. Sci.* **375**, 20160292 (2017).
- ¹⁴J. B. Borges, H. S. Ramos, R. A. Mini, O. A. Rosso, A. C. Frery, and A. A. F. Loureiro, “Learning and distinguishing time series dynamics via ordinal patterns transition graphs,” *Applied Mathematics and Computation* **362**, 124554 (2019).
- ¹⁵N. P. Subramanyam, R. V. Donner, D. Caron, G. Panuccio, and J. Hyttinen, “Causal coupling inference from multivariate time series based on ordinal partition transition networks,” *Nonlinear Dynamics* (in review), arXiv preprint 2010.00948.
- ¹⁶C. Bandt and B. Pompe, “Permutation entropy: A natural complexity measure for time series,” *Phys. Rev. Lett.* **88**, 174102 (2002).
- ¹⁷J. M. Amigó, K. Keller, and V. A. Unakafova, “Ordinal symbolic analysis and its application to biomedical recordings,” *Phil. Trans. R. Soc. A* **373**, 20140091 (2014).
- ¹⁸M. Zanin, “Forbidden patterns in financial time series,” *Chaos* **18**, 013119 (2008).
- ¹⁹M. Barreiro, A. C. Martí, and C. Masoller, “Inferring long memory processes in the climate network via ordinal pattern analysis,” *Chaos* **21**, 013101 (2011).
- ²⁰F. Takens, “Detecting strange attractors in turbulence,” in *Dynamical Systems and Turbulence, Warwick 1980*, Lecture Notes in Mathematics, Vol. 898, edited by D. Rand and L.-S. Young (Springer, New York, 1981) pp. 366–381.
- ²¹J. M. Amigó, S. Zambrano, and M. A. F. Sanjuán, “True and false forbidden patterns in deterministic and random dynamics,” *Europhys. Lett.* **79**, 50001 (2007).
- ²²J. M. Amigó, S. Zambrano, and M. A. F. Sanjuán, “Combinatorial detection of determinism in noisy time series,” *Europhys. Lett.* **83**, 60005 (2008).
- ²³O. A. Rosso, L. C. Carpi, P. M. Saco, M. G. Ravetti, H. A. Larrendo, and A. Plastino, “The Amigó paradigm of forbidden/missing patterns: a detailed analysis,” *Eur. Phys. J. B* **85**, 419 (2012).
- ²⁴A. M. Kowalski, M. T. Martin, A. Plastino, O. A. Rosso, and M. Casas, “Distances in probability space and the statistical complexity setup,” *Entropy* **13**, 1055–1075 (2011).
- ²⁵R. López-Ruiz, H. L. Mancini, and X. Calbet, “A statistical measure of complexity,” *Phys. Lett. A* **209**, 321–326 (1995).
- ²⁶O. A. Rosso, H. A. Larrendo, M. T. Martin, A. Plastino, and M. A. Fuentes, “Distinguishing noise from chaos,” *Phys. Rev. Lett.* **99**, 154102 (2007).
- ²⁷H. Lange, O. A. Rosso, and M. Hauhs, “Ordinal pattern and statistical complexity analysis of daily stream flow time series,” *Eur. Phys. J. Spec. Top.* **222**, 535–552 (2013).
- ²⁸M. Martin, A. Plastino, and O. A. Rosso, “Statistical complexity and disequilibrium,” *Phys. Lett. A* **311**, 126–132 (2003).
- ²⁹J. E. Bates and H. K. Shepard, “Measuring complexity using information fluctuation,” *Phys. Lett. A* **172**, 416–425 (1993).
- ³⁰L. da F. Costa, F. A. Rodrigues, G. Travieso, and P. R. V. Boas, “Characterization of complex networks: A survey of measurements,” *Advances in Physics* **56**, 167–242 (2007).
- ³¹A. A. B. Pessa and H. V. Ribeiro, “Characterizing stochastic time series with ordinal networks,” *Phys. Rev. E* **100**, 042304 (2019).
- ³²A. Kowalski, M. Martin, A. Plastino, and O. Rosso, “Bandt-pompe approach to the classical-quantum transition,” *Physica D* **233**, 21–31 (2007).
- ³³M. Riedl, A. Müller, and N. Wessel, “Practical considerations of permutation entropy,” *Eur. Phys. J. Spec. Top.* **222**, 249–262 (2013).
- ³⁴O. A. Rosso, L. Zunino, D. G. Pérez, A. Figliola, H. A. Larrendo, M. Garavaglia, M. T. Martín, and A. Plastino, “Extracting features of gaussian self-similar stochastic processes via the bandt-pompe approach,” *Phys. Rev. E* **76**, 061114 (2007).
- ³⁵M. Martin, A. Plastino, and O. A. Rosso, “Generalized statistical complexity measures: Geometrical and analytical properties,” *Physica A* **369**, 439–462 (2006).
- ³⁶R. L.-Ruiz, H. Mancini, and X. Calbet, “A statistical measure of complexity,” in *Concepts and Recent Advances in Generalized Information Measures and Statistics*, edited by A. M. Kowalski, R. D. Rossignoli, and E. M. F. Curado (Bentham Science Publishers, 2010) pp. 147–168.
- ³⁷Y. Zou, R. V. Donner, and J. Kurths, “Analyzing long-term correlated stochastic processes by means of recurrence networks: Potentials and pitfalls,” *Phys. Rev. E* **91**, 022926 (2015), 1409.3613.
- ³⁸O. E. Rössler, “An equation for continuous chaos,” *Phys. Lett. A* **57**, 397–398 (1976).
- ³⁹P. L. Read, M. J. Bel, D. W. Johnson, and R. M. Small, “Quasi-periodic and chaotic flow regimes in a thermally driven, rotating fluid in a nulus,” *Journal of Fluid Mechanics* **238**, 599–632 (1992).
- ⁴⁰Y. Zou, M. Thiel, M. Romano, P. Read, and J. Kurths, “Recurrence analysis of quasiperiodicity in experimental fluid data,” *Eur. Phys. J. Spec. Top.* **164**, 23–33 (2008).
- ⁴¹M. Thiel, M. C. Romano, P. L. Read, and J. Kurths, “Estimation of dynamical invariants without embedding by recurrence plots,” *Chaos* **14**, 234–243 (2004).
- ⁴²A. L. Goldberger, L. A. N. Amaral, L. Glass, J. M. Hausdorff, P. C. Ivanov, R. G. Mark, J. E. Mietus, G. B. Moody, C.-K. Peng, and H. E. Stanley, “Physiobank, physiotoolkit, and physionet,” *Circulation* **101**, e215–e220 (2000).

- ⁴³M. Small, D. Yu, J. Simonotto, R. G. Harrison, N. Grubb, and K. Fox, “Uncovering non-linear structure in human ecg recordings,” *Chaos, Solitons & Fractals* **13**, 1755 – 1762 (2002).